Applied Catalysis B: Environmental 313 (2022) 121450

Contents lists available at ScienceDirect

Applied Catalysis B: Environmental

journal homepage: www.elsevier.com/locate/apcatb

Single-particle exciton-initiated photo-catalytic reaction mapping on defective cuprous oxide

Xinyue Xiang, Wei Huang, Yi He *

National Collaborative Innovation Center for Nuclear Waste and Environmental Safety, School of National Defence Science & Technology, Southwest University of Science and Technology, Mianyang 621010, PR China

ARTICLE INFO

Keywords:
Exciton
Photocatalysis
Single-particle imaging
Cuprous oxide
Singlet oxygen

ABSTRACT

Although the exciton-triggered photocatalysis has recently been confirmed, so far it is limited to the low-dimensional semiconductors, and the characterization approaches are impossible to image and characterize the photo-catalytic reaction on single semiconductor photocatalysts. Herein by combining dark-field microscopy with 3, 3′, 5, 5′-tetramethylbenzidine as the chromogenic probe, we visually map the exciton-initiated photo-catalytic reaction on defective Cu_2O microcrystals in real time at the single-particle level. Single-particle imaging results reveal the heterogeneity in reactivity among different individuals and at different regions within the same microcrystal. Moreover, the reaction rate constant of this photocatalytic reaction is determined as well. The theoretical simulations suggest that the introduction of Mn^{2+} can modulate the electronic structure and enhance the oxygen affinity of Cu_2O, facilitating the production of $^1O_2$. This high spatio-temporal-resolution imaging approach is general, which is also appropriate for investigating the exciton effects on Fe^{2+}-doped Cu_2O microcrystals.

1. Introduction

Semiconductor-involved photocatalysis is a promising avenue for converting the solar energy conversion to chemical energy [1,2]. As a typical p-type semiconductor photocatalyst, cuprous oxide (Cu_2O) has a high carrier mobility and suitable energy band position, which is explored for water splitting, carbon dioxide reduction, organic synthesis, and pollution treatment [3–6]. Among these efforts, investigations on the band structure design and photo-generated charge carrier separation are considered as the key to pursuing effective photo-catalysis [7]. However, the traditional perspectives focused on the charge-carrier dominated redox processes are demonstrated to be incomprehensive because they omit the inherent Coulomb interactions between photo-generated electrons and holes [8]. Recently, excitons or bound electron-hole pairs have been reported to directly participate in the photocatalysis processes [9]. In the exciton-based photocatalysis, the molecular oxygen is activated to generate highly reactive singlet oxygen ($^1O_2$) via energy transfer process [10]. Defect engineering (introduction of doping and vacancy) is a major way for improving the exciton effect on photocatalytic processes, which is related to the light absorption, electronic state, and adsorption active site of O_2 [9,11]. Despite the findings of the exciton-triggering photocatalysis, the reported photocatalysts are limited to the low-dimensional semiconductors such as two-dimensional black phosphorus, heptazine-based melon, defective Bi_3O_4Br and BiOBr nanosheets [12–16]. Seldom efforts are devoted to explore the excitonic effects in Cu_2O microcrystal photocatalyst.

The neglect of the excitonic effect in the Cu_2O microcrystal photocatalyst is mainly ascribed to the great challenge for characterizing excitonic properties. Currently, photoluminescencent spectroscopy, ultrafast transient absorption and electron spin resonance are three complementary approaches for investigating excitonic properties [9]. Such methods are ensemble-averaged and ex-situ as well as depends on the test conditions, which only offers the information about the average excitonic properties of many photocatalysts under non-photocatalytic conditions. These drawbacks prevent the comprehensive understanding of the excitonic effect on semiconductors for photocatalysis. As a result, it is of great importance to in situ study the excitonic properties of semiconductor photocatalysts at the single-particle level under reaction conditions to reveal the heterogeneous and dynamic reaction activity.

Dark-field microscopy (DFM) has emerged as a convenient and powerful optical tool for studying dynamic reactions on single plasmonic nanomaterials (silver and gold nanoparticles) due to their strong

* Corresponding author.
E-mail address: yhe2014@126.com (Y. He).

https://doi.org/10.1016/j.apcatb.2022.121450
Received 19 March 2022; Received in revised form 14 April 2022; Accepted 24 April 2022
Available online 4 May 2022

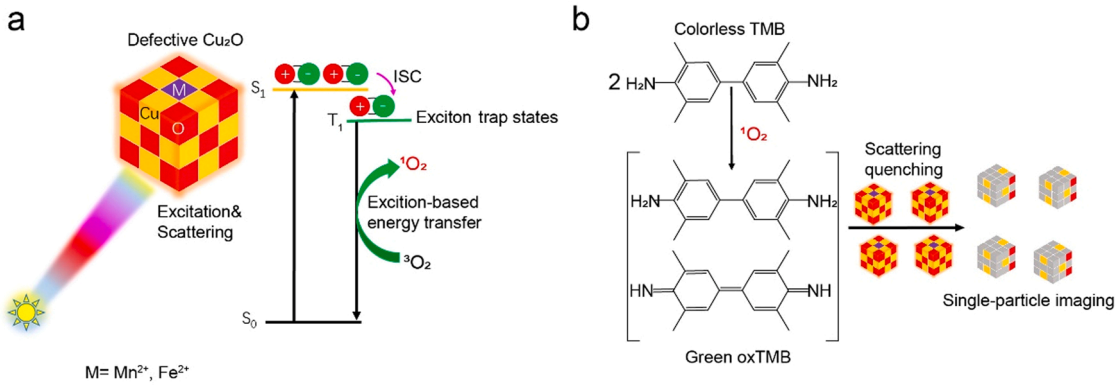

Fig. 1. Principle of the single-particle imaging method. (a) Schematic illustration of exciton-involved photocatalytic process on defective Cu_2O photocatalysts for generation of $^1O_2$. (b) Schematic of imaging the photocatalytic chromogenic reactions between $^1O_2$ and TMB on single defective Cu_2O crystal using dark-field microscopy.

scattering efficiencies [17,18]. Recently, our group has proved the capacity of DFM for directly imaging the ion exchange and chemical conversion process in single Cu_2O microcrystals based on the Mie scattering [19–21]. These examples extend the application range of DFM from noble metal nanoparticles to microscale semiconductor photocatalysts. Moreover, it has been demonstrated that the $^1O_2$ from the exciton-based photocatalysis can oxidize the 3, 3′, 5, 5′-tetramethylbenzidine (TMB) to yield green oxidation-state TMB (oxTMB) [15]. Despite the excellent visible-light absorption properties of oxTMB, there is no attempt to utilize TMB as the probe to real-time image the exciton-triggered photo-catalytic reactions at the single-particle level.

In this work, we firstly employ the DFM to visually map the exciton-initiated photo-catalytic reaction on single Mn^{2+}or Fe^{2+}-doped Cu_2O microcrystals in real time and in situ. Our single-particle DFM imaging of the photo-catalytic reaction is based on the characteristic Mie scattering of defective Cu_2O and a catalytic chromogenic reaction. As illustrated schematically in Fig. 1, defective Cu_2O microcrystals can effectively scatter the red light under the illumination of broadband white light, showing a red color under DFM observation (Fig. 1a). The incident white light simultaneously excites the defective Cu_2O microcrystals to generate singlet excitons (S1) from the Coulomb interactions of holes and electrons. The resulting excitons in S1 partially pass to the triplet state (T1) via intersystem crossing (ISC), which is quenched by energy transfer to dissolved oxygen to produce $^1O_2$. The resulting $^1O_2$ on defective Cu_2O can oxidize the colorless TMB to green oxTMB with a strong optical absorption in the red light region, inducing the quenching of the red scattering light from single defective Cu_2O photocatalyst (Fig. 1b). The doping of Mn^{2+} or Fe^{2+} introduces a surface defective state on the Cu_2O microcrystal that reduces the singlet-triplet energy gap and stabilizes the triplet exciton, promoting the production of $^1O_2$. Benefiting from the good combination of scattering, photo-catalytic and absorption properties, this DFM imaging technique is capable of resolving the detailed catalytic kinetics of the excitonic processes of defective Cu_2O photocatalysts at the single-particle level. We observe the heterogeneous exciton-based photocatalytic activity on different individual defective Cu_2O microcrystals. Additionally, we can directly differentiate distinct catalytic activity at different regions on single defective Cu_2O photocatalyst. These results pave the way for fundamental understanding of the excitonic effect in the photocatalysis field and guiding the design of high-efficient semiconductor photocatalysts.

2. Methods

2.1. Single-particle DFM imaging experiments and analyses

The exciton-initiated photo-catalytic reaction is imaged by a dark-field microscope as previously described [19], using the Olympus optical microscope coupled to an oil-immersion dark-field condenser (1.2 < numerical aperture (N. A.) < 1.4). The 100 W halogen lamp as the incident white light source is used to excite the defective Cu_2O microcrystals and produce Mie scattering light. The DFM images of the defective Cu_2O microcrystals are taken using a 40 X water-immersion objective lens (N. A. = 0.75) and captured by a true-color cooled charge-coupled device (CCD) camera at the exposure time of 50 ms. The corresponding scattering spectra are collected by a fiber spectrophotometer (EK2000, Shanghai Choptics). 10 μL Mn^{2+}-doped Cu_2O dispersion is placed onto a clean glass slide. Subsequently, 10 μL TMB reaction solution (1 mM, pH =3) is added. The resulting mixture is covered by a glass coverslip (18 mm × 18 mm). The DFM images of the photo-catalytic reaction on single defective Cu_2O microcrystals are collected at different time, and the RGB values are analyzed by Image J software.

2.2. Calculation details

The theoretical calculations are performed on the CASTEP packages. The generalized gradient approximation (GGA) and Perdew-Burke-Ernzerhof (PBE) are employed for various calculations to describe the exchange-correlation energy. The cutoff energy for the plane-wave basis is set as 381 eV. In addition, we select the ultrasoft pseudopotentials with the On-the-fly generated (OTFG) algorithm. For the k-point settings, we utilize the medium (6 ×6 ×6) quality for the energy minimizations. The atomic configurations of Cu_2O and Mn^{2+}-doped Cu_2O are relaxed with the maximum residual forces of 0.05 eV $Å^{-1}$.

3. Results and discussion

3.1. Single-particle mapping on Mn^{2+}-doped Cu_2O microcrystals

The Mn^{2+}-doped Cu_2O microcrystals are prepared via a cationic exchange strategy [22]. The X-ray diffraction (XRD) patterns in Fig. S1 and Fig. S2 verify the successful synthesis of cubic Mn^{2+}-doped Cu_2O. The scanning electron microscopy (SEM) images show a concave cube morphology of Mn^{2+}-doped Cu_2O with an average size of 4.2 μm, and the corresponding elemental mapping suggests a uniform distribution of Mn element (Fig. 1a). X-ray photoelectron (XPS) spectra show that two peaks at 932.7 eV correspond to Cu (I), and at 650.9 eV correspond to Mn (II) (Fig. S3 and S4), respectively. The mass loading of Mn in Mn^{2+}-doped Cu_2O microcrystal is detected to be 0.1 wt% using atomic absorption spectroscopy (AAS). The diffuse reflectance spectra (DRS) of Mn^{2+} doped Cu_2O is very similar to that of Cu_2O (Fig. S5), indicating that the doping process does not alter the band gap of Cu_2O. In contrast, a significant photoluminescence (PL) quenching of Cu_2O is found in the Mn^{2+} doped Cu_2O, which is ascribed to the enhanced singlet-triplet

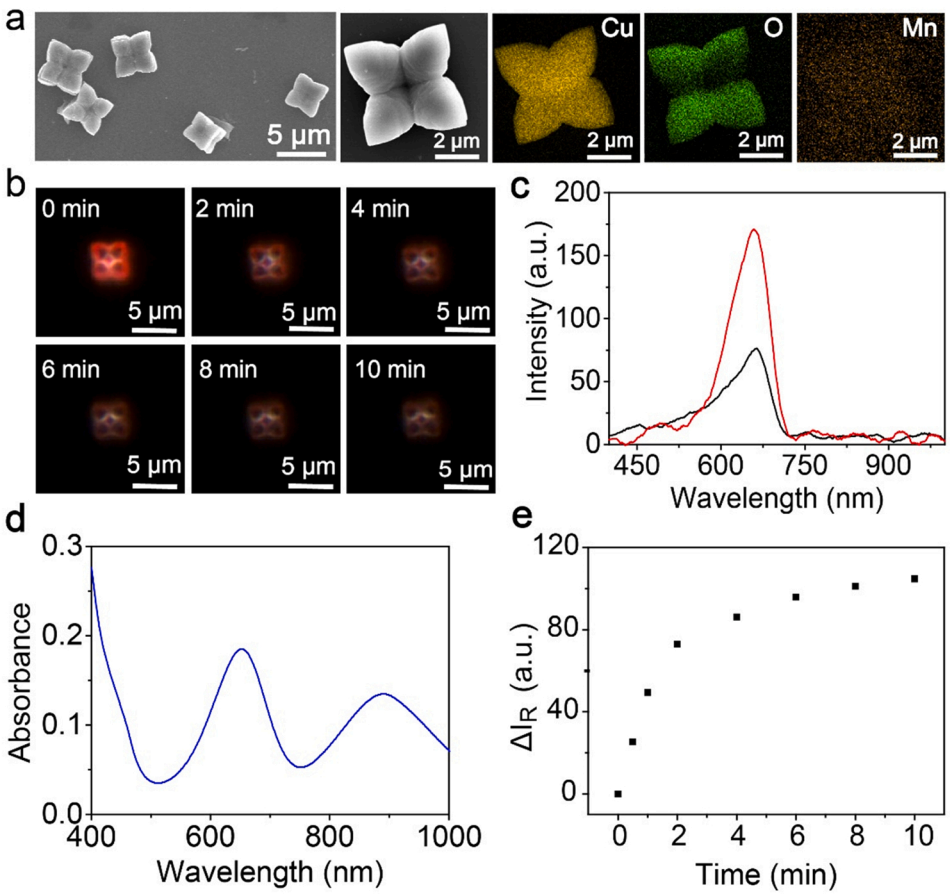

Fig. 2. Single-particle exciton-based photocatalytic reaction mapping. (a) SEM and element mapping images of Mn^{2+}-doped Cu_2O microcrystals. (b) Time-resolved DFM images of single Mn^{2+}-doped Cu_2O microcrystal at 0.5 mM TMB, pH = 3 and 50 ms imaging rate. (c) Scattering spectra of Mn^{2+}-doped Cu_2O microcrystal before (red line) and after photocatalytic reaction. (d) UV–vis absorption spectrum of the supernatant of the Mn^{2+}-doped Cu_2O-TMB reaction system. (e) The change of R value (ΔI_R) of the DFM image as a function of reaction time. $\Delta I_R = I_{R0} - I_{Rt}$, where I_{R0} and I_{Rt} are the R values of the DFM image at time zero and t, respectively.

intersystem crossing (Fig. S6). To monitor the exciton-based photocatalytic reaction of single Mn^{2+}-doped Cu_2O, we use the TMB as the probe to determine $^1O_2$. As shown in Fig. 2b and c, the Mn^{2+}-doped Cu_2O microcrystal selectively scatters red light, and a scattering peak at around 658 nm is found. The red Mn^{2+}-doped Cu_2O microcrystal becomes dark at t = 2 min, suggesting that the exciton-based photocatalytic reaction occurs, which generates the oxTMB for quenching the scattering light due to good spectra overlapping between them (Figs. 2c and 2d). As the photocatalytic reaction proceeds, the scattering intensity of the Mn^{2+}-doped Cu_2O microcrystal continuously decreases (Fig. 2b). The final scattering intensity of Mn^{2+}-doped Cu_2O microcrystal-TMB reaction system after reaction is no more than two-fifths of original Mn^{2+}-doped Cu_2O microcrystal, as shown in the final 10-min scattering spectrum (Fig. 2c). These results clearly indicate that the present DFM imaging strategy can real-time and visually track the exciton-based photocatalytic reaction on single Mn^{2+}-doped Cu_2O microcrystal.

Our assumption that the exciton-triggered photocatalytic reaction of Mn^{2+}-doped Cu_2O microcrystal induces the generation of $^1O_2$ that oxidizes TMB to green oxTMB is confirmed by a series of complementary characterizations. First, the dark Mn^{2+}-doped Cu_2O microcrystal because of the adsorption of oxTMB recoveries the red color after washing with water (Fig. S7). In the UV–vis absorption spectrum of the supernatant of the Mn^{2+}-doped Cu_2O microcrystal-TMB photocatalytic reaction system, two clear absorption bands at 655 nm and 891 nm attributed to the oxTMB are observed (Fig. 2d and Fig. S8) [14], demonstrating the existence of the oxidation process of TMB and scattering light quenching of Mn^{2+}-doped Cu_2O microcrystal due to the absorption of oxTMB. Second, there is no apparent color alteration of pristine Cu_2O microcrystal in the presence of TMB under DFM irradiation (Fig. S9), implying that the doping of Mn^{2+} is imperative for inducing the exciton-triggered photocatalytic reaction. XPS measurements show that the valence states of Cu and Mn in Mn^{2+}-doped Cu_2O microcrystal after reaction are not different from that of the original crystal (Fig. S3 and S4). Third, ascorbic acid and L-tryptophan as the antioxidant and $^1O_2$ scavenger are observed to suppress TMB oxidation, pointing out that $^1O_2$ is major oxidation species within the photocatalytic reaction (Fig. S10). Finally, the electron-spin resonance (ESR) spectra of the Mn^{2+}-doped Cu_2O microcrystal dispersion are recorded by using 2, 2, 6, 6-tetramethyl-4-piperidinol-N-oxyl (TEMP) and 5, 5-dimethyl-1-pyrroline N-oxide (DMPO) as the trapping agents under visible light illumination. As depicted in Fig. S11, the typical 1:1:1 triplet signals of a spin adduct obtained from TEMP and $^1O_2$ emerge, confirming the generation of $^1O_2$ via the exciton-triggered photocatalytic process. In comparison, the negligible sextet ESR signal generated from DMPO-OOH (a spin adduct derived from DMPO and superoxide anion) verifies that the traditional carrier-based charge transfer process is not related to the observed photocatalytic reaction on Mn^{2+}-doped Cu_2O microcrystal (Fig. S12). On the basis of the above findings, we can affirm that the doping of Mn^{2+} is the key factor for producing energy-transfer process from exciton in T_1 and molecular O_2, initiating the photo-catalytic reaction that oxidizes TMB to green oxTMB and thus quenching the scattering light of the Mn^{2+}-doped Cu_2O microcrystal, leading to the scattering intensity decrease (Fig. 2c).

To describe more clearly the color change of Mn^{2+}-doped Cu_2O microcrystal, we plot the change of R value (ΔI_R) of the DFM image during the photo-catalytic process (Fig. 2e). The evolutions of ΔI_R are able to be divided into two stages. At the first stage, the ΔI_R increases dramatically from the start to 2 min, indicating the fast oxidation of TMB by $^1O_2$. The second stage is from 2 min to 10 min. The ΔI_R changes slowly and reaches a maximum around 10 min. Clearly, the ΔI_R can be employed for quantitatively tracking the exciton-based photocatalytic reaction on the single Mn^{2+}-doped Cu_2O microcrystal.

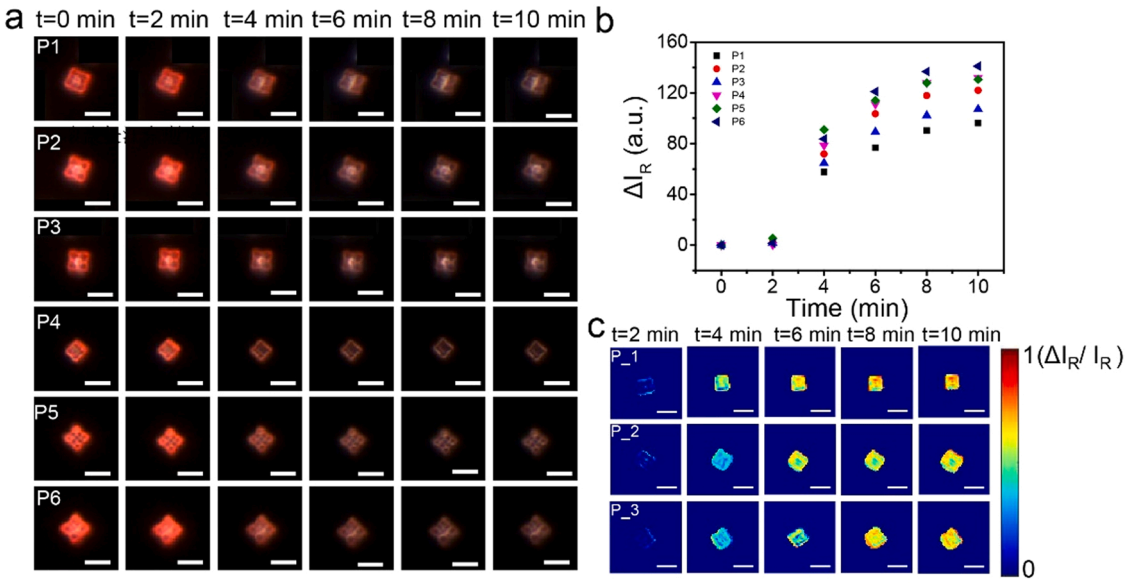

Fig. 3. Heterogeneous reactivity in the exciton-based photocatalysis. (a) DFM images of six Mn^{2+}-doped Cu_2O microcrystals (P1 to P6) as a function of reaction time (reaction conditions: 0.5 mM TMB and pH 3) and (b) the corresponding scattering intensity change (ΔI_R) versus the reaction time. (c) Spatial distribution of the average change ratio of R value due to the optical absorption of the photocatalytic product oxTMB on the three Mn^{2+}-doped Cu_2O microcrystals (P_1 to P_3). Scale bars, 5 μm.

3.2. *Inter-and intra-particle heterogeneous photo-catalytic reactivity*

The high temporal-spatial evolution of the present DFM imaging method allows us to reveal intrinsically heterogeneous photo-catalytic reactivity, which is challenging to explore in ensemble characterizations. Fig. 3a plots the time-lapsed DFM images of six Mn^{2+}-doped Cu_2O microcrystals marked by P1-P6 in the presence of TMB solution. As the exciton-based photocatalysis occurs, the six red Mn^{2+}-doped Cu_2O microcrystals fades when exposed to TMB solution under DFM irradiation. The corresponding time-dependent ΔI_R varies for different Mn^{2+}-doped Cu_2O microcrystals (Fig. 3b), revealing the distinct photo-catalytic reactivity for different particles. For instance, P6 and P2 have a similar size. The equilibrium ΔI_R of P6 is greater than that of P2, pointing to the high photo-catalytic reactivity of P6. In addition, although the size of P4 is significantly smaller than that of P1, the photocatalytic activity of P4 is obviously better than P1. These activity maps illustrate that there is a particle-to-particle activity heterogeneity, which is not dependent on the size of Mn^{2+}-doped Cu_2O microcrystal. The statistical analysis further demonstrates the heterogeneity among different Mn^{2+}-doped Cu_2O microcrystals (Fig. S13).

Since in situ DFM also allows to monitor the photo-catalytic reaction on the surface of single Mn^{2+}-doped Cu_2O microcrystals, we examine the spatial distribution of the average change ratio of R value ($\Delta I_R/I_R$) from three representative microcrystals, labeled with P_1, P_2, and P_3. As shown in Fig. 3c, the photo-catalytic reactivity of P_1 is mainly located at the upper left corner of the microcrystal, whereas the edge and corner of P_2 has larger values of $\Delta I_{Rt}/I_{R0}$ than its facet. In addition, for the P_3, the facet also shows a remarkable photo-catalytic activity. Accordingly, the large heterogeneity of single Mn^{2+}-doped Cu_2O microcrystal in activity is clear at different surface regions, corroborating the requirement for single-particle level studying. The resulting inter-particle heterogeneous photo-catalytic reactivity among different Mn^{2+}-doped Cu_2O microcrystals and intra-particle activity heterogeneity within the single Mn^{2+}-doped Cu_2O microcrystal is ascribed to the inhomogeneous doping of Mn (Fig. S14 and S15) [23–26].

3.3. *Photo-catalytic kinetic analysis*

The exciton-based photocatalysis process involves two steps: the generation of $^1O_2$ and TMB oxidation reaction. In the step 1, the photocatalytic reaction induced energy transfer between triplet-state exciton and dissolved oxygen generates the $^1O_2$ within picoseconds [16]. Compared with the photoreaction step, the chemical reaction is usually slow because of the limitation of reactant diffusion and reaction

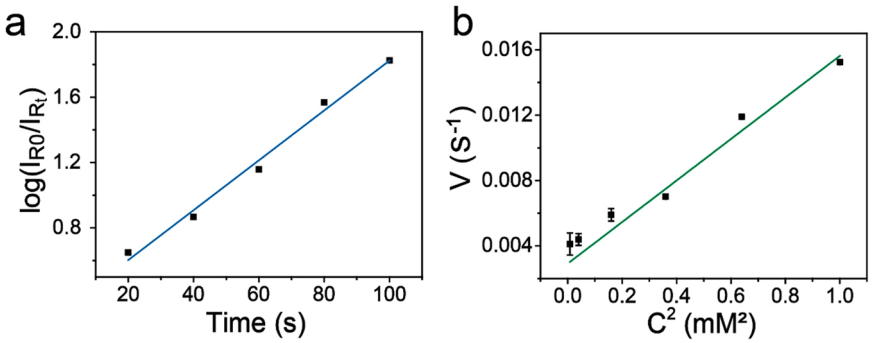

Fig. 4. Study of the rate constant of the exciton-based photo-catalytic reaction. (a) The logarithm of the ratio of R value at time zero and t as a function of reaction time for single Mn^{2+}-doped Cu_2O at 1 mM TMB and pH 3. (b) Linear correlation between the initial rates of TMB oxidation (v) and the square of TMB concentration (C^2).

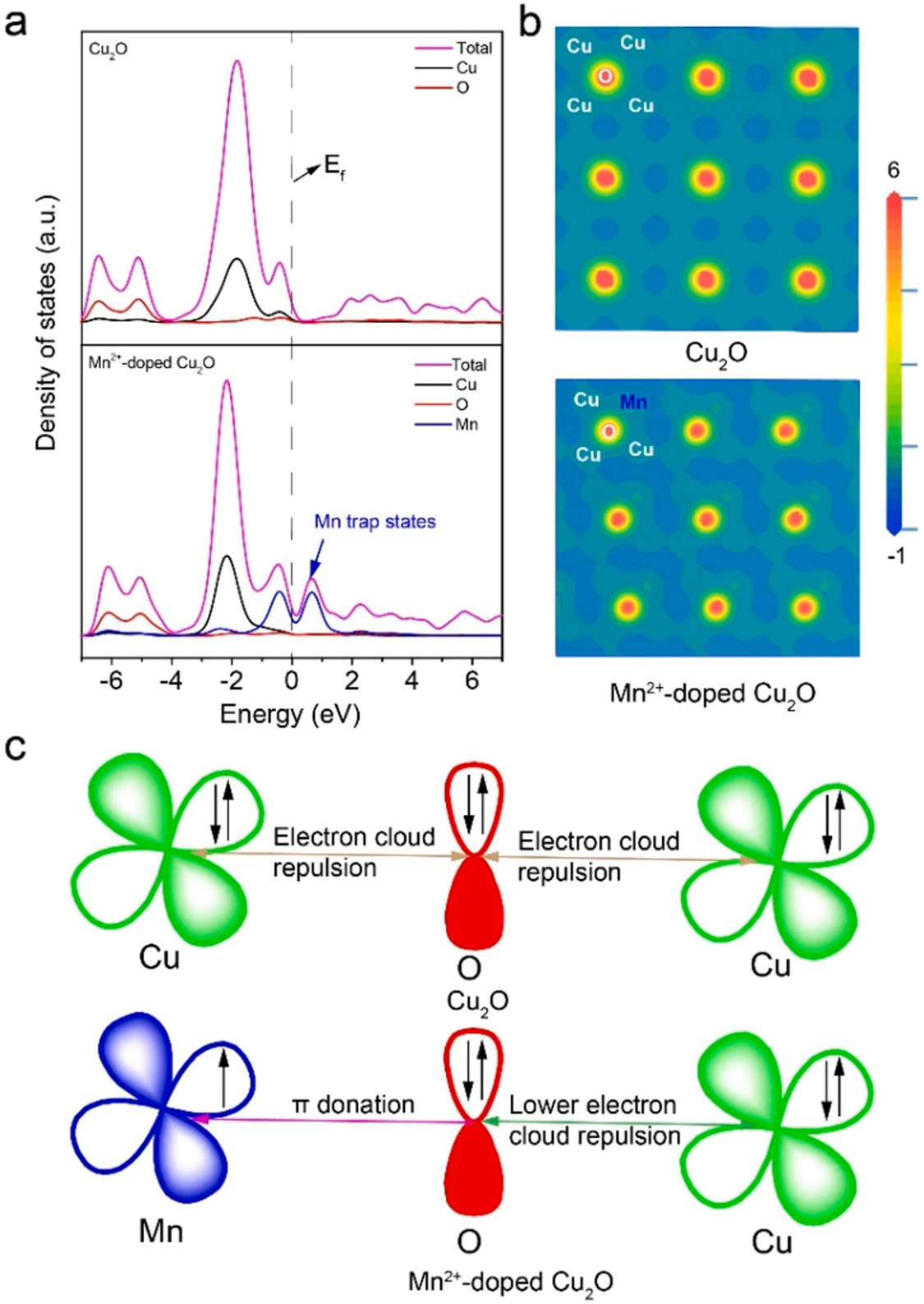

Fig. 5. Theoretical calculation for Cu_2O and Mn^{2+}-doped Cu_2O. (a) Calculated density of states and (b) electron density map for Cu_2O and Mn^{2+}-doped Cu_2O. (c) Schematic description of the electron cloud coupling of Cu-O-Cu and Mn-O-Cu in Cu_2O and Mn^{2+}-doped Cu_2O.

pathways. Accordingly, the chemical oxidation of TMB by $^1O_2$ is the rate-limiting step. To analyze the photo-catalytic kinetic of the single Mn^{2+}-doped Cu_2O microcrystal, we suppose that each Mn^{2+}-doped Cu_2O microcrystal can be considered as a micro-scale luminous source. The oxidation product of TMB (oxTMB) that consists of TMB and TMB radical absorbs the scattering light of Mn^{2+}-doped Cu_2O microcrystal, which follows the Lambert-Beer law. The oxTMB is formed by the following equation:

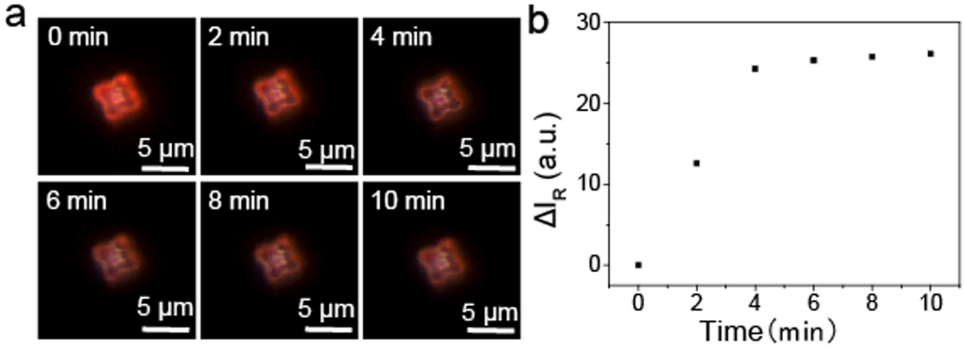

Fig. 6. Demonstration of the generality of the imaging strategy. (a) Time-lapsed DFM images of single Fe^{2+}-doped Cu_2O microcrystal at 0.5 mM TMB, pH = 3 and 50 ms imaging rate. (b) The change of R value (ΔI_R) of the DFM image versus reaction time.

$$2TMB + O_2 \xrightarrow[h\nu]{Mn^{2+}-doped\ Cu_2O} oxTMB + H_2O \quad (1)$$

According to the Eq. (1), the initial rate of TMB oxidation (v) can be written as.

$$v = dC_{oxTMB}/dt \quad (2)$$

where C_{oxTMB} and t are the concentration of oxTMB and reaction time. The C_{oxTMB} is estimated by the absorbance (A)-like equation:

$$A = \log (I_{R0}/I_{Rt}) = k_0\, C_{oxTMB} \quad (3)$$

where k_0 is a constant. Eq. (3) predicts that v is proportional to dlog $(I_{R0}/I_{Rt})/dt$. Assuming the rate-limiting step of TMB oxidation by $^1O_2$ is a second-order reaction because the dissolved O_2 is excessive, the rate equation can be also expressed as.

$$v = k_1\, C_{TMB}^2 \quad (4)$$

where k_1 is the rate constant. Based on Eqs. (2–4), the observed reaction rate constant (k_{obs}) is further calculated by.

$$dA/dt = d\log (I_{R0}/I_{Rt})/dt = k_0\, k_1\, C_{TMB}^2 = k_{obs}\, C_{TMB}^2 \quad (5)$$

Fitting the experimental data in Fig. 4a and b with Eqs. (3 and 5), two good linear correlations are obtained, demonstrating the occurrence of the second-order reaction. Also, the k_{obs} is estimated to be 0.01525 $s^{-1}\cdot mM^{-2}$. The capacity of this in-situ DFM imaging method for calculating k_{obs} permits us to quantitatively describe the exciton-initiated photo-catalytic reaction and screen high-performance photocatalysts.

3.4. Theoretical simulations

To decipher the underlying role of Mn doping on the exciton-based photocatalysis within Mn^{2+}-doped Cu_2O, we utilize the density-function theory (DFT) to calculate the electronic structures of Cu_2O before and after doping Mn^{2+}. Fig. 5a shows the density of states (DOS) for Cu_2O and Mn^{2+}-doped Cu_2O. After Mn^{2+} doping, the Mn^{2+} in Cu^+ site provides a trap state between conduction and valence bands of Cu_2O, which serves as singlet exciton trap states to decrease the energy gap between singlet and triplet states. This trap state boosts the ISC process for production of more triplet excitons [13]. Meanwhile, the doping of Mn^{2+} also influences the interaction between dissolved oxygen and Cu_2O microcrystal. The valence electronic configuration of Cu^+ is $3d^{10}$. The corresponding d-orbitals are fully occupied. Therefore, there is a strong electron cloud repulsion between Cu^+ and O^{2-} (Figs. 5b and 5c), which can not accommodate excess electrons from dissolved O_2, resulting in weak oxygen adsorption on Cu_2O.

The electron density maps visualize the interactions between Cu^+ and O^{2-} (Fig. 5b). In the pristine Cu_2O, the electron-rich region is derived from O atoms due to the electron donation of Cu atoms. After incorporation of Mn^{2+}, the low electron density is found because Mn^{2+} with an unfilled $3d^5$ valence electronic configuration interacts with the bridging O^{2-} via π-donation (Figs. 5b and 5c). Such interaction alleviates the electron cloud repulsion of Cu^+ and O^{2-}, promoting the adsorption of dissolved O_2 to yield $^1O_2$ via exciton-based energy transfer process. These theoretical results confirm that the doping of Mn^{2+} not only introduces a singlet-exciton trapping state but also improves the dissolved O_2 adsorption on the surface of Cu_2O microcrystal for manipulating ISC process and surface chemical sorption of O_2 to generate $^1O_2$.

3.5. Imaging the photo-catalytic reaction on Fe^{2+}-doped Cu_2O

In order to illustrate the generality of the imaging strategy for studying the exciton-based photocatalysis, we dope Fe^{2+} with unfilled $3d^6$ electron configuration into Cu_2O microcrystals using the same experimental conditions. The structure of the resulting Fe^{2+}-doped Cu_2O microcrystals is investigated by transmission electron microscopy (TEM) (Fig. S16). Fig. 6a displays the time-sequential DFM images of single Fe^{2+}-doped Cu_2O microcrystal in the presence of TMB. At the beginning, the Fe^{2+}-doped Cu_2O microcrystal displays a red color, confirming that the doping of Fe^{2+} does not alter the scattering property of the Cu_2O microcrystal. Subsequently, the red Fe^{2+}-doped Cu_2O microcrystal possesses a similar fading phenomenon as the reaction time prolongs to 6 min, clearly demonstrating the existence of $^1O_2$ from the exciton-based photo-catalytic reaction on the surface of Fe^{2+}-doped Cu_2O microcrystal. Besides, the Fe^{2+}-doped Cu_2O microcrystal shows a fast photo-catalytic reaction kinetics with respect to Mn^{2+}-doped Cu_2O microcrystal, because the equilibration time of Fe^{2+}-doped Cu_2O microcrystal is approximatively 4 min that is lower than that of Mn^{2+}-doped Cu_2O microcrystal (~ 10 min) (Fig. 2e and Fig. 6b). Based on the above results, we believe that the doping strategy for the formation of defective Cu_2O is a general avenue to start up the exciton-based photocatalysis and boost the production of $^1O_2$.

4. Conclusions

In summary, we have proposed the DFM as a powerful method to in situ visually monitor the exciton-initiated photo-catalytic reaction on single defective Cu_2O microcrystal under reaction conditions by using TMB as the probe. Single-particle DFM imaging confirms that the doping of Mn^{2+} can promote the yield of triplet-excitons for $^1O_2$ via energy transfer process. By recording the change of R values from the DFM images, we successfully reveal the inter-and intra-particle heterogeneous photo-catalytic reactivity of defective Cu_2O microcrystals at the single-particle level. The photo-catalytic kinetic is also analyzed, and the corresponding reaction rate constant is determined, which is useful for quantitative description of the exciton-based photo-catalysis. Theoretical simulation results imply that the introduction of Mn^{2+} results in the generation of singlet exciton trap states and improve the adsorption

capacity for dissolved oxygen on Cu_2O microcrystals, therefore favoring the exciton-triggered photo-catalysis for forming $^1O_2$. The generality of this DFM imaging strategy is further demonstrated for investigating the exciton-based photo-catalysis on single Fe^{2+}-doped Cu_2O microcrystal. Arising from the high contrast and spatial resolution of DFM, it opens possibilities to supply a general method for better understanding the excitonic effect-dominated photocatalysis at the single-particle level and development of advanced photo-catalysts.

CRediT authorship contribution statement

Xinyue Xiang conducted most of the experiments and analyzed the data. Wei Huang performed some experiments and analyzed the data. Yi He supervised the project, designed the experimental setup, and wrote the manuscript. All authors reviewed the manuscript and approved the final version of the manuscript for submission.

Declaration of Competing Interest

The authors declare no competing financial interests.

Acknowledgements

The support of this research by the Key Research and Development Project of Science & Technology Department of Sichuan Province (Grant No. 2021YFS0316) is gratefully acknowledged.

Appendix A. Supporting information

Supplementary data associated with this article can be found in the online version at doi:10.1016/j.apcatb.2022.121450.

References

[1] L. Zhang, J. Ran, S.-Z. Qiao, M. Jaroniec, Characterization of semiconductor photocatalysts, Chem. Soc. Rev. 48 (2019) 5184–5206.
[2] T. Hisatomi, J. Kubota, K. Domen, Recent advances in semiconductors for photocatalytic and photoelectrochemical water splitting, Chem. Soc. Rev. 43 (2014) 7520–7535.
[3] Y. Xin, K. Yu, L. Zhang, Y. Yang, H. Yuan, H. Li, L. Wang, J. Zeng, Copper-based plasmonic catalysis: recent advances and future perspectives, Adv. Mater. 33 (2021), 2008145.
[4] Y.A. Wu, I. McNulty, C. Liu, K.C. Lau, Q. Liu, A.P. Paulikas, C.-J. Sun, Z. Cai, J. R. Guest, Y. Ren, Facet-dependent active sites of a single Cu_2O particle photocatalyst for CO_2 reduction to methanol, Nat. Energy 4 (2019) 957–968.
[5] R. Chen, S. Pang, H. An, J. Zhu, S. Ye, Y. Gao, F. Fan, C. Li, Charge separation via asymmetric illumination in photocatalytic Cu_2O particles, Nat. Energy 3 (2018) 655–663.
[6] A. Paracchino, V. Laporte, K. Sivula, M. Grätzel, E. Thimsen, Highly active oxide photocathode for photoelectrochemical water reduction, Nat. Mater. 10 (2011) 456–461.
[7] T.-N. Chen, J.-C. Kao, X.-Y. Zhong, S.-J. Chan, A.S. Patra, Y.-C. Lo, M.H. Huang, Facet-specific photocatalytic activity enhancement of Cu_2O polyhedra functionalized with 4-ethynylanaline resulting from band structure tuning, ACS Cent. Sci. 6 (2020) 984–994.
[8] A. Raja, A. Chaves, J. Yu, G. Arefe, H.M. Hill, A.F. Rigosi, T.C. Berkelbach, P. Nagler, C. Schüller, T. Korn, Coulomb engineering of the bandgap and excitons in two-dimensional materials, Nat. Commun. 8 (2017) 15251.
[9] H. Wang, W. Liu, X. He, P. Zhang, X. Zhang, Y. Xie, An excitonic perspective on low-dimensional semiconductors for photocatalysis, J. Am. Chem. Soc. 142 (2020) 14007–14022.
[10] H. Wang, S. Jiang, W. Liu, X. Zhang, Q. Zhang, Y. Luo, Y. Xie, Ketones as molecular co-catalysts for boosting exciton-based photocatalytic molecular oxygen activation, Angew. Chem. Int. Ed. 132 (2020) 11186–11193.
[11] S. Bai, N. Zhang, C. Gao, Y. Xiong, Defect engineering in photocatalytic materials, Nano Energy 53 (2018) 296–336.
[12] Y. Li, H. Wang, X. Zhang, S. Wang, S. Jin, X. Xu, W. Liu, Z. Zhao, Y. Xie, Exciton-mediated energy transfer in heterojunction enables infrared light photocatalysis, Angew. Chem. Int. Ed. 133 (2021) 13001–13006.
[13] D. Zhang, P. Wang, J. Wang, Y. Li, Y. Xia, S. Zhan, Tailoring of electronic and surface structures boosts exciton-triggering photocatalysis for singlet oxygen generation, Proc. Natl. Acad. Sci. U.S.A. 118 (2021), e2114729118.
[14] H. Wang, S. Chen, D. Yong, X. Zhang, S. Li, W. Shao, X. Sun, B. Pan, Y. Xie, Giant electron-hole interactions in confined layered structures for molecular oxygen activation, J. Am. Chem. Soc. 139 (2017) 4737–4742.
[15] H. Wang, X. Sun, D. Li, X. Zhang, S. Chen, W. Shao, Y. Tian, Y. Xie, Boosting hot-electron generation: exciton dissociation at the order–disorder interfaces in polymeric photocatalysts, J. Am. Chem. Soc. 139 (2017) 2468–2473.
[16] H. Wang, D. Yong, S. Chen, S. Jiang, X. Zhang, W. Shao, Q. Zhang, W. Yan, B. Pan, Y. Xie, Oxygen-vacancy-mediated exciton dissociation in BiOBr for boosting charge-carrier-involved molecular oxygen activation, J. Am. Chem. Soc. 140 (2018) 1760–1766.
[17] C. Novo, A.M. Funston, P. Mulvaney, Direct observation of chemical reactions on single gold nanocrystals using surface plasmon spectroscopy, Nat. Nanotechnol. 3 (2008) 598–602.
[18] G.L. Liu, Y.-T. Long, Y. Choi, T. Kang, L.P. Lee, Quantized plasmon quenching dips nanospectroscopy via plasmon resonance energy transfer, Nat. Methods 4 (2007) 1015–1017.
[19] W. Huang, L. Yu, Y. Zhu, H. Yu, Y. He, Single-particle imaging of anion exchange reactions in cuprous oxide, ACS Nano 15 (2021) 6481–6488.
[20] W. Huang, H. Li, L. Yu, Y. Lin, Y. Lei, L. Jin, H. Yu, Y. He, Imaging adsorption of iodide on single Cu_2O microparticles reveals the acid activation mechanism, J. Hazard. Mater. 420 (2021), 126539.
[21] L. Yu, J. Wang, Z. Liu, Y. Lin, W. Huang, Y. He, Imaging and manipulating the conversion from single cuprous oxide microparticles to single metal hydroxide microstructures, Inorg. Chem. 60 (2021) 19421–19428.
[22] F. Li, G.-F. Han, J.-P. Jeon, T.J. Shin, Z. Fu, Y. Lu, J.-B. Baek, Surface electronic modulation with hetero-single atoms to enhance oxygen evolution catalysis, ACS Nano 15 (2021) 11891–11897.
[23] J.B. Sambur, T.-Y. Chen, E. Choudhary, G. Chen, E.J. Nissen, E.M. Thomas, N. Zou, P. Chen, Sub-particle reaction and photocurrent mapping to optimize catalyst-modified photoanodes, Nature 530 (2016) 77–80.
[24] M. Hesari, X. Mao, P. Chen, Charge carrier activity on single-particle photo (electro) catalysts: Toward function in solar energy conversion, J. Am. Chem. Soc. 140 (2018) 6729–6740.
[25] N.M. Andoy, X. Zhou, E. Choudhary, H. Shen, G. Liu, P. Chen, Single-molecule catalysis mapping quantifies site-specific activity and uncovers radial activity gradient on single 2D nanocrystals, J. Am. Chem. Soc. 135 (2013) 1845–1852.
[26] X. Ye, M.R. Jones, L.B. Frechette, Q. Chen, A.S. Powers, P. Ercius, G. Dunn, G. M. Rotskoff, S.C. Nguyen, V.P. Adiga, Single-particle mapping of nonequilibrium nanocrystal transformations, Science 354 (2016) 874–877.